

**Key Words:** micro-macro modelling, fibre-reinforced composites, finite element modelling

*Chapter 1*

# INTRODUCTION TO FINITE ELEMENT ANALYSIS AND RECENT DEVELOPMENTS

*B. D. Reddy and A. T. McBride* \*

Centre for Research in Computational and Applied Mechanics  
University of Cape Town, 7701 Rondebosch, South Africa

## **Abstract**

Fibre-reinforced composite materials are composed of dispersed fibrous materials (e.g. glass, natural materials, polyethylene, Kevlar, etc.) set within a continuous polymer matrix.

The primary benefits of fibre-reinforced composites over traditional engineering materials comes from their impressive strength-to-weight ratio and the ability to design the microstructure so as to optimise their macrostructural properties. These advantageous properties were first exploited by the space and aerospace industries. Currently fibre-reinforced composites are an ubiquitous component of modern production and design for a range of products spanning exotic high technology components to more mundane household items.

The focus of this chapter is on the second of the aforementioned advantages of fibre-reinforced composites over traditional materials: the ability to tailor the macroscopic properties by designing the microstructural configuration, and the role of the finite element method as a computational tool which makes such multi-scale modelling possible. We emphasise how this bottom-up approach changes the traditional computational modelling

---

\*Email address for correspondence: [daya.reddy@uct.ac.za](mailto:daya.reddy@uct.ac.za)

perspective where the response of the material is generally formulated upon macroscopic considerations. The role of the finite element method in micro-macro approaches is described, and the resulting numerical considerations presented and discussed. Also discussed are the statistical techniques needed to interpret the resulting data. Some background to the relevant solid mechanics and the finite element method is presented before discussing the topics of relevance.

## 2. Introduction

Fibre-reinforced composites have become an integral component of many modern products. The ability to specialise the design of the composite material for its end purpose presents the designer with various challenges such as choosing the optimal fibre volume fraction, fibre orientation and fibre type. Computational modelling allows designers to use virtual product prototyping to assist them in the design process. The objective of this chapter is to provide a clear overview of modern multi-scale computational modelling methodologies for fibre-reinforced composites.

By means of introduction, Section 2.1. presents a brief overview of several of the key features of fibre-reinforced composites. Thereafter, a discussion of the multi-scale modelling methodology within the context of the finite element method is given. The Introduction concludes with an overview of the use of multi-scale modelling to determine material properties at the macro-scale. These issues will be explored in more depth in subsequent sections.

### 2.1. Features of fibre-reinforced composites

Fibre-reinforced composite materials are composed of dispersed fibrous materials (e.g. glass, natural materials, polyethylene, Kevlar, etc.) set within a continuous polymer matrix. The fibrous material is generally of a higher strength than the matrix material. The matrix serves to bond the fibres together, to transfer the stresses due to loading to the fibres, and to protect the fibres against environmental factors. The resulting composite has desirable properties that neither the fibre nor the matrix possess alone.

A fibre-reinforced composite part is generally a laminate composed of layers of stacked fibre-matrix material that are then bonded together. The fibres can either be continuous strands or chopped segments. The orientation of the fibres in each of the layers and the fibre volume ratio can be adjusted to tailor the composite for its final application.

The high degree of flexibility in the design process allows fibre-reinforced composites to be used in a wide range of applications, including aircraft and military components, automotive components, a large variety of sporting goods, construction materials, and in medical and dental applications (the reader is referred to Mallick [1993] for extensive details).

Fibre-reinforced composites do however have some potential drawbacks. These include high cost, brittle behaviour, susceptibility to deformation under long-term loads, ultra-violet degradation, temperature and moisture effects, and a lack of design codes.

## 2.2. Computational modelling of fibre-reinforced composites

Computational modelling is now an integral part of the modern design process. It has greatly reduced design times by allowing virtual prototyping to supplement expensive experimental testing. At the heart of any computational model lies a mathematical model predicting the response of the media to applied loading. An understanding of these, often complex, mathematical models and the tools used to solve them numerically is critical for a designer to correctly interpret the results of the model. A computational model is simply that, a model, and its limitations should be understood.

An objective of this chapter is to provide greater insight into one such computational modelling methodology, termed multi-scale modelling. Multi-scale modelling allows one to imbed micro-scale phenomena within a macro-scale model using a process known as homogenisation. For an excellent detailed overview of computational micro-mechanics the reader is referred to Zohdi and Wriggers [2004]. Multi-scale modelling based upon homogenisation has been an active area of research for at least 20 years, but the major works that led to this field becoming well understood both mathematically and computationally have appeared within the last decade (the reader is referred to the recent review article by Geers et al. [2009] and references therein).

There has been significant work on the multi-scale modelling of fibre-reinforced composites; examples include the contributions by [Belsky et al., 1995, Feyel and Chaboche, 2000, Sansalone et al., 2006] with specific focus on topics such as fracture and failure [Xia et al., 2001, Xia and Curtin, 2001, González and LLorca, 2006], viscoplasticity [Feyel, 1999], biomechanics [Maceri et al., 2010], amongst others. Their heavy computational cost, however, is one of the main reasons prohibiting their inclusion in commercial finite element software currently. This cost must be seen in perspective however; a simulation at the macro-scale that directly includes the detail of the micro-scale without the aid of some sort of homogenisation procedure is computationally intractable for all but the simplest of problems.

The multi-scale modelling approach is presented here within the framework of the finite element method (see, for example, Hughes [1987] and Zienkiewicz and Taylor [2005] which has a chapter dedicated to multi-scale modelling, amongst numerous others, for extensive details). The finite element method is a widely used and mature tool for solving the systems of partial differential equations that typically describe the behaviour of solid and fluid continuous media.

A typical finite element simulation proceeds as follows. The domain of the problem is divided into a set of non-overlapping regions termed elements. The solution of the problem is then sought in the approximate form of simple functions such as polynomials over each element. The weak or integral form of the governing equations is used to construct the approximate problem, which is linear if the problem is linear. The contributions from each element are assembled into a global matrix that represents, loosely, the stiffness of the system. A key step in this procedure is prescribing the material or constitutive model, that is, the relationship between the stress the material experiences and the resulting deformation it undergoes.

Conventional macro-scale finite element simulations assume that the material can be described by measurable macroscopic material properties. Typical examples for solids in-

clude materials that are modelled as elastic, viscoelastic, plastic, and viscoplastic. The presentation in this chapter will be confined to linear elastic materials.

Multi-scale modelling makes no such assumptions about the underlying constitutive model. Rather, essential features of the micro-scale model are directly linked to the macro-scale model via a homogenisation process. The constitutive relationship at the macro-scale is thus allowed to develop from the microscopic behaviour. This necessitates the solution of a separate micro-scale model at selected points such as quadrature points, in the macroscopic body. The objective of the micro-macro approach is to obtain effective material properties that characterise, in an averaged sense and at the macroscopic level, the underlying microscopic details.

The size of the micro-scale model is determined via the concept of a representative volume element (RVE). The RVE should represent the smallest sample at the micro-scale capable of capturing the behaviour accurately. If the RVE is too small then a biased and unrepresentative view of the microstructure is obtained. If the RVE is too large then computational effort is wasted. The procedure to determine the optimal RVE size is based upon physical measurement and numerical tests. Methodologies to determine the optimal RVE size have been presented by various authors (see, for example, Kouznetsova [2002] and Zohdi and Wriggers [2001]) and will be elaborated on further in this work.

To clarify issues, consider the example of a thermo-mechanically loaded plate presented by Ozdemir et al. [2008]. The plate is made of boron fibre reinforced aluminium (see Figure 1). The fibres are unidirectionally oriented parallel to the  $z$ -axis. The plate is clamped on its side surfaces and exposed to a rapidly increasing uniform temperature and mechanical load on the top surface. A plane-strain assumption is used to model the plate. The unidirectional orientation of the uniform fibres in this case makes the determination of the RVE straightforward: it is simply a volume surrounding a fibre cross-section. The ratio of the depth of the plate to the length of the RVE is approximately 182, indicating a clear separation of scale. Figure 2 shows the evolution of temperature and plastic strain after 10.0 s of simulation. A key motivation for adopting such a multi-scale model is to be able to capture the highly anisotropic plastic strain distribution shown at point B. One could imagine the extraordinary computational power that would be required to directly account for each fibre directly within the macro-scale model, as would be the case using a conventional macroscopic finite element approach.

The linkage between the scales in the multi-scale framework is based on two key properties. Firstly, the micro-scale features are assumed to be significantly smaller than the macro-scale; that is, we have a separation of scales. Secondly, there is an equivalence between the work done at the micro- and macro-scales. These principles will be elaborated upon further in later sections.

### 2.3. Determining material properties using a multi-scale framework

A key application of the multi-scale modelling formulation discussed previously is to determine numerically the appropriate macro-scale material parameters for use in a macro-scale model, see for example Zohdi and Wriggers [2001]. The solution of the macro-scale model can then be performed using mature finite element software in a fraction of the time that it would take to do a full multi-scale simulation. The motivation for adopting this strategy

would be to capture as closely as possible the micro-scale material parameters, for use at the macro-scale.

Consider the example of a non-woven needle-punched microstructure consisting of randomly distributed fibres, as shown in Figure 3. The macro-scale response would be isotropic as there is no preferred fibre direction and, if the deformations were sufficiently small, could be approximated as a linear elastic material. Using this methodology, the designer of the fibre-reinforced composite could use a multi-scale methodology to determine, for example, the optimal fibre fraction and fibre type so as to satisfy various criteria. In this approach, a series of micro-scale finite element simulations are performed and the results analysed using statistical tools to determine the material properties. A rigorous procedure to perform such a series of micro-scale test has been presented by Zohdi and Wriggers [2001] and will be elaborated on further in this chapter. The implementation of this procedure within a commercial finite element package and a discussion of the results will also be presented.

**Notation.** We will use boldface italic letters to denote vectors and tensors. We adopt the summation convention for repeated indices, unless stated otherwise. Most often, vectors are denoted by lowercase boldface italic letters, and second-order tensors, or  $3 \times 3$  matrices, by lowercase boldface Greek letters. Fourth-order tensors are usually denoted by uppercase boldface italic letters. We will make use of a Cartesian coordinate system with an orthonormal basis  $\{e_1, e_2, e_3\}$ . Where it is necessary to show components of a vector or a tensor, these will always be relative to the orthonormal basis  $\{e_1, e_2, e_3\}$ . Throughout this work we will identify a second-order tensors  $\tau$  with a  $3 \times 3$  matrix. We will always use  $a_i$ ,  $1 \leq i \leq 3$ , to denote the components of the vector  $a$ , and  $\tau_{ij}$ ,  $1 \leq i, j \leq 3$ , the components of the second-order tensor  $\tau$ . With the basis defined, the action of the second-order tensor  $\tau$  on the vector  $a$  may be represented in the form

$$\tau a = \tau_{ij} a_j e_i.$$

The scalar products of two vectors  $a$  and  $b$ , and of two second-order tensors (or matrices)  $\sigma$  and  $\tau$ , are denoted by  $a \cdot b$  and  $\sigma : \tau$  and have the component representations

$$a \cdot b = a_i b_i, \quad \sigma : \tau = \sigma_{ij} \tau_{ij}.$$

The magnitudes of a vector  $a$  and a second-order tensor  $\tau$  are defined by

$$|a| = (a \cdot a)^{\frac{1}{2}}, \quad |\tau| = (\tau : \tau)^{\frac{1}{2}}.$$

The tensor product  $a \otimes b$  of two vectors  $a$  and  $b$  is a second-order tensor defined by the relation

$$(a \otimes b)c = (b \cdot c)a \quad \forall c.$$

Viewed as a matrix, we have the representation

$$a \otimes b = ab^T.$$

Since we will be working with a fixed basis, there is little point in making a formal distinction between the tensor  $\tau$  and the  $3 \times 3$  matrix of its components, so that unless otherwise stated,  $\tau$  will represent the tensor *and* the matrix of its components. With this understanding,

it is merely necessary to point out that all the usual matrix operations such as addition, transposition, multiplication, inversion, and so on, apply to tensors, and the standard notation is used for these operations. Thus, for example,  $\tau^T$  and  $\tau^{-1}$  are, respectively, the transpose and inverse of the tensor (or matrix)  $\tau$ . Every second-order tensor  $\tau$  may be additively decomposed into a deviatoric part  $\tau^D$  and a spherical part  $\tau^S$ ; these are defined by

$$\tau^S = \frac{1}{3} (\text{tr}\tau)I, \quad \tau^D = \tau - \frac{1}{3} (\text{tr}\tau)I,$$

so that

$$\tau = \tau^D + \tau^S.$$

The invariants of a tensor are defined by

$$\begin{aligned} I_1 &= \text{tr}\tau = \tau_{ii} = \tau_1 + \tau_2 + \tau_3, \\ I_2 &= \frac{1}{2} \{ (\text{tr}\tau)^2 - \text{tr}\tau^2 \} = \frac{1}{2} (\tau_{ii}\tau_{jj} - \tau_{ij}\tau_{ji}) = \tau_1\tau_2 + \tau_2\tau_3 + \tau_3\tau_1, \\ I_3 &= \det\tau = \tau_1\tau_2\tau_3. \end{aligned}$$

Here,  $\tau_1$ ,  $\tau_2$ , and  $\tau_3$ , are the eigenvalues of  $\tau$ . The eigenvalues  $\tau_i$  of a matrix  $\tau$  are called the *principal components* of  $\tau$ .

**Scalar, vector, and tensor fields.** The gradient of a scalar field  $\phi(x)$  is denoted by  $\nabla\phi$  and is the vector defined by

$$\nabla\phi = \frac{\partial\phi}{\partial x_i} e_i.$$

The divergence  $\text{div}u$  and gradient  $\nabla u$  of a vector field  $u(x)$  are respectively a scalar and a second-order tensor field, defined by

$$\begin{aligned} \text{div}u &= \frac{\partial u_i}{\partial x_i}, \\ (\nabla u)_{ij} &= \frac{\partial u_i}{\partial x_j}. \end{aligned}$$

The divergence  $\text{div}\tau$  of a second-order tensor  $\tau$  is a vector with components

$$(\text{div}\tau)_i = \frac{\partial \tau_{ij}}{\partial x_j}.$$

### 3. Continuum mechanics and linear elasticity

The continuum approach to the description of mechanical behaviour starts with the assumption that a body at the macroscopic level may be regarded as composed of material that is continuously distributed. Such a body occupies a region of three-dimensional space. The region occupied by the body will of course vary with time as the body deforms. The region occupied by the body in the reference configuration at the time  $t = 0$  is denoted by  $\Omega$ , and a material point may be identified by the position vector  $x$ . The properties and the behaviour of the body can be described in terms of functions of position  $x$  in the body and time  $t$ . The motion is orientation-preserving; that is, the *Jacobian*  $J$ , defined by  $J = \det(\partial y_i / \partial x_j)$ ,

must be positive. Hence, every element of nonzero volume in  $\Omega$  is mapped to an element of nonzero volume in  $\Omega_t$ .

Introduce the *displacement* vector  $u$  by

$$u = y(x, t).$$

The strain tensor, defined by

$$\eta(u) = \frac{1}{2} [\nabla u + (\nabla u)^T + (\nabla u)^T \nabla u],$$

measures deformation in the body, and is zero if the body undergoes a rigid body motion. The components  $\eta_{ij}$  may be interpreted as follows:  $\eta_{11}$  equals half the net *change in length* (squared) of a material fiber originally oriented so that it points in the  $x_1$  direction, and the other two diagonal components of the strain are interpreted in a similar way. The off-diagonal component  $\eta_{12}$  gives a measure of the *change in angle* between two fibres originally at right angles to each other and oriented so that they were in the  $x_1$  and  $x_2$  directions, and the remaining off-diagonal components are interpreted in a similar way. The diagonal components are referred to as *direct strains*, while the off-diagonal components are referred to as *shear strains*.

**Infinitesimal strain.** A body is said to undergo infinitesimal deformation if the displacement gradient is sufficiently small so that nonlinear terms can be neglected. When this is the case, we may replace the strain tensor  $\eta$  by the infinitesimal strain  $\varepsilon$ , which is defined by

$$\varepsilon = \frac{1}{2} (\nabla u + (\nabla u)^T) \tag{1}$$

For infinitesimal deformations the change in volume per unit volume is

$$\frac{\Delta V}{V} = \text{div } u. \tag{2}$$

An incompressible material is one which is unable to undergo any volume change. For bodies comprising such materials, the displacement must therefore satisfy the condition

$$\text{div } u = 0. \tag{3}$$

**Balance of momentum; stress.** Suppose that the body is subjected to a system of forces, which are of two kinds. There is the *body force*  $b(x, t)$ , which represents the force per unit reference volume exerted on the material point  $x$  at time  $t$  by agencies external to the body; gravity is a canonical example, the body force in this case being  $\rho g e$ , where  $g$  is the gravitational acceleration,  $\rho$  is the mass density, and  $e$  is the unit vector pointing in the downward vertical direction. The second kind of force acting on any surface in the body or on its boundary is the *surface traction*,  $s_n$ , which denotes the force per unit area acting on a surface with outward unit normal vector  $n$ . Cauchy's Theorem states that there exists a second-order tensor or matrix  $\sigma$  with the property that the surface traction on a surface with outward unit normal  $n$  is given by

$$\sigma n = s_n.$$

The tensor  $\sigma$  is known as the Cauchy stress.

**BALANCE OF LINEAR MOMENTUM.** The total force acting on an arbitrary part  $\Omega'_t$  of the body  $\Omega_t$  is equal to the rate of change of the linear momentum of  $\Omega'_t$ ; expressed in terms of integrals over the reference configuration,

$$\int_{\Omega'} \rho \ddot{u} dx = \int_{\Omega'} b dx + \int_{\Gamma'} s_n ds. \quad (4)$$

An immediate consequence of balance of linear momentum is that the stress satisfies the equation of motion

$$\operatorname{div} \sigma + b = \rho \ddot{u}.$$

For situations in which all the given data are independent of time, the response of the body will also be independent of time. In this case the equation of motion becomes the *equation of equilibrium*

$$\operatorname{div} \sigma + b = \mathbf{0}.$$

These equations are valid in the current configuration, but since infinitesimal deformations are assumed throughout, it suffices to solve these equations on the reference domain.

**BALANCE OF ANGULAR MOMENTUM.** The total moment acting on  $\Omega'_t$  is equal to the rate of change of the angular momentum of  $\Omega'_t$ ; expressed in terms of integrals over the reference configuration,

$$\int_{\Omega'} x \wedge \rho \ddot{u} dx = \int_{\Omega'} x \wedge b dx + \int_{\Gamma'} x \wedge s_n ds.$$

An immediate consequence of balance of angular momentum is that the stress tensor is symmetric: that is,

$$\sigma^T = \sigma. \quad (5)$$

In summary then, the principles of balance of linear and angular momentum are

$$\operatorname{div} \sigma + b = \rho \ddot{u}, \quad (6)$$

$$\sigma^T = \sigma. \quad (7)$$

**Boundary conditions.** In addition to the governing equations, which must be satisfied at every point in the body, it is also necessary to specify a set of boundary conditions. These are of two kinds: a Dirichlet or essential boundary condition, in which the displacement is specified to be equal to a prescribed value on a part  $\Gamma_D$  of the boundary  $\Gamma$ ; and a Neumann or natural boundary condition, in which the surface traction is specified on the complementary part  $\Gamma_N$  of the boundary. Thus the boundary conditions are

$$\begin{aligned} u &= \bar{u} \quad \text{on } \Gamma_D, \\ \sigma n &= \bar{s} \quad \text{on } \Gamma_N. \end{aligned} \quad (8)$$

It is possible that no natural boundary condition is specified, in which case  $\Gamma_D$  is the entire boundary  $\Gamma$ . But the converse, that is, of no essential boundary condition, is not considered as such a body could not be in equilibrium, not being fixed at any point on its boundary.

**Linearly elastic materials.** A body is *linearly elastic* if the stress depends linearly on the infinitesimal strain, that is, if the stress and strain are related to each other through an equation of the form

$$\sigma = C\varepsilon, \quad (9)$$

where  $C$ , called the *elasticity tensor*. If the density  $\rho$  and the elasticity tensor  $C$  are independent of position, the body is said to be *homogeneous*. The constitutive equation (9) has the component form

$$\sigma_{ij} = C_{ijkl}\varepsilon_{kl}.$$

It is often the case that materials possess preferred directions or symmetries. For example, timber can be regarded as an orthotropic material, in the sense that it possesses particular constitutive properties along the grain and at right angles to the grain of the wood. The greatest degree of symmetry is possessed by a material that has no preferred directions; that is, say, its response to a force is independent of its orientation. This property is known as isotropy, and a material with such a property is called *isotropic*. For an isotropic material the constitutive equation (9) can be written in terms of only two material constants. The stress-strain relation in this case is given by

$$\sigma = \lambda(\text{tr}\varepsilon)I + 2\mu\varepsilon.$$

For the purpose of interpreting the moduli, we recall that any second-order tensor  $\tau$  may be written in the form

$$\tau = \tau^D + \tau^S,$$

where the deviatoric and spherical parts  $\tau^D$  and  $\tau^S$  of  $\tau$  are defined, respectively, by

$$\tau^D = \tau - \frac{1}{3}(\text{tr}\tau)I, \quad \tau^S = \frac{1}{3}(\text{tr}\tau)I. \quad (10)$$

The constitutive equation can then be written in the *uncoupled form*

$$\sigma^D = 2\mu\varepsilon^D, \quad (11)$$

$$\sigma^S = \lambda(\text{tr}\varepsilon)I^S + 2\mu\varepsilon^S = 3\left(\lambda + \frac{2}{3}\mu\right)\varepsilon^S. \quad (12)$$

The scalar  $\mu$  is also known as the *shear modulus* (for reasons that are evident from (11)), while the material coefficient  $K \equiv \lambda + \frac{2}{3}\mu$  is known as the *bulk modulus* because it measures the ratio between the spherical stress and volume change. Thus an alternative pair of elastic coefficients to the Lamé moduli is  $\{\mu, K\}$ . Note that the shear modulus is often denoted by  $G$ , especially in the engineering literature.

Yet another important alternative pair of material coefficients arises from direct consideration of the behaviour of the length of an elastic rod when it is subjected to a uniaxial stress. Suppose that the Cartesian axes are aligned in such a way that an isotropic elastic rod lies parallel to the  $x_1$ -axis and is subjected to a uniform stress with  $\sigma_{11} \neq 0$  and all other components being zero. The effect will be that the rod experiences only direct strains, on account of its isotropy. We are interested here first in the ratio  $\sigma_{11}/\varepsilon_{11}$  and second in

the ratio  $\varepsilon_{22}/\varepsilon_{11}$ , or, equivalently,  $\varepsilon_{33}/\varepsilon_{11}$ . The associated material coefficients are known, respectively, as *Young's modulus* and *Poisson's ratio*:

$$\begin{aligned} \text{Young's modulus } E &= \frac{\sigma_{11}}{\varepsilon_{11}}, \\ \text{Poisson's ratio } \nu &= -\frac{\varepsilon_{22}}{\varepsilon_{11}}. \end{aligned}$$

Thus Young's modulus measures the slope of the stress–strain curve and is analogous to the stiffness of a spring, while Poisson's ratio measures lateral contraction. The constitutive relation (9) can be expressed in terms of  $E$  and  $\nu$  as follows:

$$\varepsilon = E^{-1}[(1 + \nu)\sigma - \nu(\text{tr}\sigma)I].$$

Finally, the bulk and shear moduli  $K$  and  $G$  are given in terms of  $E$  and  $\nu$  by

$$K = \frac{E}{3(1 - 2\nu)}, \quad G = \frac{E}{2(1 + \nu)}. \quad (13)$$

**Weak formulation of the problem of elasticity** With a view to using the finite element method to obtain solutions to the problem for elastic bodies, it is necessary to convert the boundary value problem (7) to what is known as a weak formulation. To this end, let  $w$  be an arbitrary displacement which satisfies the homogeneous essential boundary condition; that is,

$$w = \mathbf{0} \quad \text{on } \Gamma_D. \quad (14)$$

Now, take the scalar product of the equilibrium equation (7)<sub>1</sub> with  $w$  and integrate this equation over the domain  $\Omega$ : this gives

$$\int_{\Omega} \text{div } \sigma \cdot w \, dV = \int_{\Omega} b \cdot w \, dV. \quad (15)$$

Next, use the divergence theorem to transform the integral on the left hand side as follows:

$$\int_{\Omega} \text{div } \sigma \cdot w \, dV = \int_{\Gamma} \sigma n \cdot w \, dA - \int_{\Omega} \sigma : \nabla w \, dV. \quad (16)$$

Now, the test function  $w$  satisfies  $w = \mathbf{0}$  on part of the boundary  $\Gamma_D$ , and on the other part  $\Gamma_N$  the surface traction is given by (8)<sub>2</sub>. Noting also Cauchy's theorem, it follows that (16) can be written as

$$\int_{\Omega} \text{div } \sigma \cdot w \, dV = \int_{\Gamma_N} \bar{s} \cdot w \, dA - \int_{\Omega} \sigma : \nabla w \, dV. \quad (17)$$

Finally, because the stress is symmetric we have  $\sigma : \nabla w = \sigma : (\nabla u + (\nabla u)^T)/2 = \sigma : \varepsilon(w)$ . Putting all of this together, the boundary value problem can now be formulated in weak form as follows: find the displacement  $u$  which satisfies  $u = \bar{u}$  on  $\Gamma_D$ , and

$$\int_{\Omega} \sigma : \varepsilon(w) \, dV = \int_{\Omega} b \cdot w \, dV + \int_{\Gamma_N} \bar{s} \cdot w \, dA \quad \text{for arbitrary displacements } w. \quad (18)$$

It can be shown that under mild conditions, the classical form (7) and the weak form (18) form are equivalent. The latter will be used to construct finite element approximations.

**Voigt notation.** It will be convenient when carrying out the finite element formulation to convert all tensorial quantities to Voigt notation. This is simply a way of expressing the components of stress and strain as column vectors, with corresponding modifications to the governing and other equations. Thus the stress and strain are written in Voigt notation as

$$\begin{aligned}\sigma &= [\sigma_{11} \ \sigma_{22} \ \sigma_{33} \ \sigma_{12} \ \sigma_{13} \ \sigma_{23}]^T, \\ \varepsilon &= [\varepsilon_{11} \ \varepsilon_{22} \ \varepsilon_{33} \ 2\varepsilon_{12} \ 2\varepsilon_{13} \ 2\varepsilon_{23}]^T.\end{aligned}\tag{19}$$

Note the factor 2 in the shear strains: this is so that the quantity  $\sigma : \varepsilon = \sigma_{ij}\varepsilon_{ij}$  can be written conveniently in Voigt notation as

$$\sigma^T \varepsilon \quad \text{or} \quad \varepsilon^T \sigma.$$

Note also that no distinction is made between the original tensor notation and Voigt notation for  $\sigma$  and  $\varepsilon$ ; the context will make clear which version is being used.

Next, consider the expression

$$[\text{div } \sigma] = \begin{pmatrix} \frac{\partial \sigma_{11}}{\partial x_1} + \frac{\partial \sigma_{12}}{\partial x_2} + \frac{\partial \sigma_{13}}{\partial x_3} \\ \frac{\partial \sigma_{21}}{\partial x_1} + \frac{\partial \sigma_{22}}{\partial x_2} + \frac{\partial \sigma_{23}}{\partial x_3} \\ \frac{\partial \sigma_{31}}{\partial x_1} + \frac{\partial \sigma_{32}}{\partial x_2} + \frac{\partial \sigma_{33}}{\partial x_3} \end{pmatrix};$$

with Voigt notation this is easily written (noting also the symmetry of  $\sigma$ ) as

$$\text{div } \sigma = \nabla_S \sigma$$

where the  $3 \times 3$  matrix  $\nabla_S$  of partial derivatives is defined by

$$\nabla_S = \begin{pmatrix} \frac{\partial}{\partial x_1} & 0 & 0 & \frac{\partial}{\partial x_2} & \frac{\partial}{\partial x_3} & 0 \\ 0 & \frac{\partial}{\partial x_2} & 0 & \frac{\partial}{\partial x_1} & 0 & \frac{\partial}{\partial x_3} \\ 0 & 0 & \frac{\partial}{\partial x_3} & 0 & \frac{\partial}{\partial x_1} & \frac{\partial}{\partial x_2} \end{pmatrix}$$

The strain can be written in terms of displacements using (1) and the same matrix  $\nabla_S$ , to give

$$\varepsilon(u) = \nabla_S^T u.$$

With these additions, the equilibrium equation becomes

$$\nabla_S \sigma + b = \mathbf{0}.$$

Finally, the elastic law for isotropic materials can be written in Voigt form as

$$\sigma = D\varepsilon = D\nabla_S u\tag{20}$$

in which the  $6 \times 6$  elasticity matrix takes the form

$$D = \frac{E}{(1+\nu)(1-2\nu)} \quad (21)$$

$$\times \begin{pmatrix} 1-\nu & \nu & \nu & 0 & 0 & 0 \\ \nu & 1-\nu & \nu & 0 & 0 & 0 \\ \nu & \nu & 1-\nu & 0 & 0 & 0 \\ 0 & 0 & 0 & (1-2\nu)/2 & 0 & 0 \\ 0 & 0 & 0 & 0 & (1-2\nu)/2 & 0 \\ 0 & 0 & 0 & 0 & 0 & (1-2\nu)/2 \end{pmatrix}. \quad (22)$$

Thus the weak form (18) becomes

$$\int_{\Omega} (\nabla_S^T w)^T D \nabla_S u \, dV = \int_{\Omega} w^T b \, dV + \int_{\Gamma_N} w^T \bar{s} \, dA. \quad (23)$$

### 3.1. The finite element method

In this section we give a brief introduction and overview of those aspects of the finite element method that are relevant to micro-macro modelling. A detailed treatment may be found, for example, in [Zienkiewicz and Taylor, 2005].

The point of departure of the finite element method is the weak formulation (23) and the Galerkin method, in which an approximate solution of the weak problem is sought. The finite element method is in turn a systematic approach to developing approximate solutions using the Galerkin method. Though the theory to be presented is applicable in three dimensions, for simplicity we will carry out the presentation in two dimensions.

The first step is to write the approximate displacement, which we denote also by  $u$ , as a linear combination of  $R$  basis or shape functions  $N_i$ ; that is,

$$u = N_1 d_1 + N_2 d_2 + \dots + N_R d_R = Nd \quad (24)$$

where the matrix  $N$  and row vector  $d$  are defined by

$$N = \begin{pmatrix} N_1 & 0 & N_2 & 0 & \dots & N_R & 0 \\ 0 & N_1 & 0 & N_2 & \dots & 0 & N_R \end{pmatrix}, \quad d = [d_1 \ d_2 \ \dots \ d_R].$$

Thus  $d$  is a  $2R \times 1$  vector with entries  $d_1, d_2$ , etc., being  $2 \times 1$  vectors of the unknown coefficients or degrees of freedom, which will need to be solved for. In the same way the arbitrary displacement  $w$  can be expressed in the form

$$w = Nq$$

where  $q$  are its degrees of freedom. Next, the strain components are obtained from

$$\varepsilon(u) = \begin{pmatrix} \partial u_1 / \partial x \\ \partial u_2 / \partial y \\ \partial u_2 / \partial x + \partial u_1 / \partial y \end{pmatrix} = \nabla_S^T u = \nabla_S^T N d = B d$$

where the  $3 \times 2R$  matrix  $B$  is given by

$$B = \nabla_S^T N$$

and whose entries are either 0 or terms of the form  $\partial N_i / \partial x_j$ . Substituting these quantities into the weak form (23), we obtain the equation

$$c^T \left( \int_{\Omega} B^T DB dV \right) d = c^T \left( \int_{\Omega} N^T \bar{b} dV + \int_{\Gamma_N} N^T \bar{s} dA \right) \quad (25)$$

or, in matrix form,

$$Kd = F$$

where the stiffness matrix  $K$  and load vector  $F$  are defined by

$$K = \int_{\Omega} B^T DB dV, \quad F = \int_{\Omega} N^T \bar{b} dV + \int_{\Gamma_N} N^T \bar{s} dA. \quad (26)$$

It can be shown that  $K$  is invertible, hence the solution to the approximate problem is found from

$$d = K^{-1}F$$

and the approximate displacement and stress can now be constructed from

$$u = Nd, \quad \sigma = DBd.$$

The finite element method is an approach that allows these steps to be carried out in a way that allows for easy construction of  $N$  and refinement of the approximation.

**The finite element mesh.** We start by partitioning the domain  $\Omega$  into a finite number  $E$  of subdomains  $\Omega_1, \Omega_2, \dots, \Omega_E$ , called *finite elements*. These elements are non-overlapping and cover  $\Omega$ , in the sense that

$$\Omega_e \cap \Omega_f = \emptyset \quad \text{for } e \neq f, \quad \bigcup_{e=1}^E \bar{\Omega}_e = \bar{\Omega}.$$

To avoid complicating matters unnecessarily, we assume that the domain  $\Omega$  is *polygonal* in two dimensions, and polyhedral in three. That is, the boundary  $\Gamma$  of  $\Omega$  is made up of straight segments in two dimensions and planar surfaces in three. This is illustrated in Figure 4 for the two-dimensional case.

It is required that every side (or surface in three dimensions) of the boundary of an element be *either* part of the boundary  $\Gamma$ , *or* a side of another element.

**Nodal points.** We next identify certain points called *nodes* or *nodal points* in the subdivided domain. Nodes are allocated at least at the vertices of elements, as shown in Figure 5(a), but in order to improve the approximation, further nodes may be introduced, for example at the midpoints of the sides of elements as shown in Figure 5(b). In any case there is a total of  $G$  nodes, say, which are numbered  $1, 2, \dots, G$  and which have position vectors  $x_1, x_2, \dots, x_G$ . The set of elements and nodes that make up the domain  $\Omega$  is called a *finite element mesh*.

**Basis functions  $N_i$ .** We construct the shape functions so that they have the following properties:

- (i) the functions  $N_i$  are *continuous*;
- (ii) there is a total of  $G$  basis functions, that is, one for each node, and each function  $N_i$  is nonzero only on those elements that are connected to node  $i$ ;
- (iii)  $N_i$  is equal to 1 at node  $i$ , and equal to zero at the other nodes:

$$N_i(x_j) = \begin{cases} 1 & \text{if } i = j, \\ 0 & \text{otherwise;} \end{cases} \quad (27)$$

- (iv) the *restriction*  $N_i^{(e)}$  of  $N_i$  to an element  $\Omega_e$  is a polynomial of degree  $k \geq 1$ .

From (iii) and (iv) it is clear that the function  $N_i^{(e)}$  defined on element  $\Omega_e$  will have the property that

$$N_i^{(e)}(x_j) = \begin{cases} 1 & \text{if } i = j, \\ 0 & \text{otherwise,} \end{cases} \quad (28)$$

$i$  and  $j$  running over all nodes in  $\Omega_e$ . We call  $N_i^{(e)}$  a *local basis function*. These ideas are illustrated in Figure 6.

It should be clear that a typical shape function  $N_i$  is built up by patching together the local basis functions  $N_i^{(e)}$  associated with node  $i$ .

To distinguish the shape functions  $N_i$  from the local shape functions  $N_i^{(e)}$ , we refer to the former as *global shape functions*.

From (24) and (27),

$$u(x_j) = \sum_{i=1}^G d_i N_i(x_j) = d_j; \quad (29)$$

that is, the coefficient  $d_j$  is simply *the value of  $u_h$  at node  $j$* .

**The approximate solution.** Recall that the stiffness matrix  $K$  is defined by

$$K = \int_{\Omega} B^T D B dV. \quad (30)$$

Now recognising that the integral in (30) can be carried out element by element, we write

$$\begin{aligned} K &= \int_{\Omega} B^T D B dV \\ &= \sum_{e=1}^E \underbrace{\int_{\Omega_e} B^{eT} D B^e dV}_{K^e} \end{aligned}$$

where  $K^e$  is the element stiffness matrix, corresponding to the contribution of element  $e$  to  $K$ .

Likewise, the load vector  $F$  can be evaluated at element level, to give

$$F = \sum_{e=1}^E F^e$$

where

$$F^e = \int_{\Omega_e} N^{eT} b \, dV + \int_{\Gamma_N^e} N^{eT} s \, dA.$$

Since  $N_i = 0$  for all elements which do not have node  $i$  as a node, clearly  $K_{ij}^{(e)} = 0$  if nodes  $i$  and  $j$  do not belong to  $\Omega_e$ . It follows that a judicious numbering of nodes will result in the matrix  $K$  having a *banded* structure in which all nonzero entries are clustered around the main diagonal. From a computational viewpoint this represents a distinct advantage.

As an example, the simplest element is one which yields piecewise-linear approximations. Such an element has nodes only at the vertices, in two and three dimensions. This is illustrated in Figures 7, in two dimensions.

This positioning of nodes ensures that if any of the sides of  $\Omega_e$  is shared with an adjacent element  $\Omega_f$ , say, the piecewise linear function formed by patching together the functions defined on  $\Omega_e$  and  $\Omega_f$  will be *continuous across the interface of these elements*.

It is convenient to adopt a local numbering system when evaluating the element stiffness matrix and load vector, in which the nodes are numbered in a counterclockwise direction, starting with node 1. Once the element stiffness matrix and load vector have been evaluated, the components can then simply be placed in the correct rows and columns of the global matrix and vector by recalling the global node numbers of the element. The process whereby  $K^{(e)}$  and  $F^{(e)}$  are computed for each element, and then added to the global matrix, is known as *assembly*.

Rather than work directly on the arbitrary element, a reference element  $\hat{\Omega}$  is set up and shape functions defined on it. These are then easily mapped onto the actual element. The reference element is a right-angled isosceles triangle (Figure 8), and the transformation

$$\begin{aligned} x &= x_1^{(e)}(1 - \xi - \eta) + x_2^{(e)}\xi + x_3^{(e)}\eta \\ y &= y_1^{(e)}(1 - \xi - \eta) + y_2^{(e)}\xi + y_3^{(e)}\eta \end{aligned}$$

or

$$x = F_e(\xi) \equiv (1 - \xi - \eta)x_1^{(e)} + \xi x_2^{(e)} + \eta x_3^{(e)}$$

maps the nodal points 1, 2, 3 of  $\hat{\Omega}$  to local nodal points 1, 2, 3 of  $\Omega_e$ , and indeed maps each point  $\xi \in \hat{\Omega}$  to a point  $x \in \Omega_e$ .

The local basis functions on  $\hat{\Omega}$  must satisfy (28), and are

$$\begin{aligned} \hat{N}_1(\xi) &= 1 - \xi - \eta, \\ \hat{N}_2(\xi) &= \xi, \\ \hat{N}_3(\xi) &= \eta; \end{aligned}$$

These functions have the property that  $\hat{N}_i = 1$  at local node  $i$ , and 0 at the other nodes. The basis function  $N_i$  formed by patching together all the local functions  $\hat{N}_i^{(e)}$  associated with node  $i$  is the two-dimensional counterpart of the “hat” function in one dimension, and is pyramidal in shape. Naturally  $N_i$  is piecewise linear, and is nonzero only on those elements that have node  $i$  as a node. This is illustrated in Figure 9.

A key stage in the implementation of the finite element method is the construction of the stiffness matrix and load vector, and these require that a number of terms be integrated,

generally over the reference element. The basis of most numerical integration schemes is the identification of selected points, known as sampling points, at which the value of the function is sampled, and the specification of a set of weights, one for each sampling point.

Suppose that integration is to be carried out over one of the reference elements  $\hat{\Omega}$ ; then if the sampling points are denoted by  $\tilde{\xi}_\ell$  ( $\ell = 1, \dots, r$ ) and the weights by  $w_\ell$  ( $\ell = 1, \dots, r$ ), a numerical integration formula of order  $r$  is defined to be a formula of the kind

$$\int_{\hat{\Omega}} f(\tilde{\xi}) d\tilde{\xi} \simeq \sum_{\ell=1}^r w_\ell f(\tilde{\xi}_\ell). \quad (31)$$

**Integration over triangles.** An integration rule of order 1 may be defined on a triangle  $\Omega_e$  by

$$\int_{\Omega_e} f(x, y) dx dy \simeq A_e f(\hat{x}, \hat{y}) \quad (32)$$

in which  $(\hat{x}, \hat{y})$  are the coordinates of the *centroid* of the triangle (Figure 10). Likewise, a rule of order 3 may be defined by

$$\int_{\Omega_e} f(x, y) dx dy \simeq \frac{1}{3} A_e \sum_{\ell=1}^3 f(\tilde{x}_\ell, \tilde{y}_\ell), \quad (33)$$

where  $(\tilde{x}_\ell, \tilde{y}_\ell)$  ( $\ell = 1, 2, 3$ ) are the coordinates of the midpoints of the sides. The rule of order 1 is exact for polynomials of degree 1, while the rule of order 3 is exact for polynomials of order 2.

## 4. Micromechanical modelling

In this section we go through the details of micro-macro modelling of a random fibre-reinforced composite. The material is assumed to be macroscopically isotropic, but it is microstructurally anisotropic as a result of the presence of fibres in a random arrangement at that scale.

The objective is to obtain effective material properties that capture, at the macroscopic level and in an averaged sense, the microscopic behaviour. These effective moduli are then used in macroscopic finite element analyses.

It is possible, via a homogenisation procedure, to find "effective" material properties at the macro-scale by creating and analysing a model of the microstructure. In this way the details of microscopic behaviour are captured in an average sense, without the need to analyse the entire structure at that scale.

Consider a representative volume element (RVE) of the body. The RVE defines a representative volume of a microscopically heterogeneous material such as a fibre-reinforced composite, a polycrystalline aggregate, or a natural material such as wood. An RVE is associated with each material point in the body, and the idea is to solve a number of boundary value problems for the RVE or microstructure, in order to obtain effective material moduli. If the material is macroscopically homogeneous, then it suffices to solve a single set of problems for a statistically representative set of RVEs, to obtain effective moduli for the macroscopic body as a whole.

In order to link the macro- and micro-problems, the boundary conditions on the RVE must ensure that the macroscopic stress power is equal to the average microscopic stress power, that is, they must satisfy Hill's condition [Hill, 1952]:

$$\underbrace{\langle \boldsymbol{\sigma}^T \boldsymbol{\varepsilon} \rangle_{\Omega}}_{\text{macroscopic stress power}} = \underbrace{\langle \boldsymbol{\sigma} \rangle_{\Omega}^T \langle \boldsymbol{\varepsilon} \rangle_{\Omega}}_{\text{microscopic stress power}} \quad (34)$$

where

$$\langle \cdot \rangle := \frac{1}{|\Omega|} \int_{\Omega} (\cdot) d\Omega \quad (35)$$

and  $\Omega$  in this instance represents the domain of the RVE.

Hill's condition is satisfied by three types of boundary conditions on the RVE, viz. linear displacement, constant traction, and periodic boundary conditions: the linear displacement and constant traction conditions are specified by

$$\mathbf{u}|_{\partial\Omega} = \boldsymbol{\mathcal{E}} \cdot \mathbf{x}, \quad (36)$$

$$\mathbf{t}|_{\partial\Omega} = \boldsymbol{\mathcal{T}} \cdot \mathbf{n}, \quad (37)$$

where  $\boldsymbol{\mathcal{E}}$  and  $\boldsymbol{\mathcal{T}}$  are constant matrices. Periodic boundary conditions are only relevant in a material with a spatially periodic microstructure and thus are not considered further in this work.

It can be shown [Zohdi and Wriggers, 2001] that the linear displacement boundary condition gives an "over-stiff" response, and the constant traction boundary condition an "under-stiff" response. These results thus give upper and lower bounds for the problem.

The analysis on the RVE will give an effective macroscopic linear elasticity tensor,  $\mathbb{E}^*$ , which relates the averages of the microscopic stress,  $\boldsymbol{\sigma}$ , and the microscopic strain,  $\boldsymbol{\varepsilon}$ :

$$\langle \boldsymbol{\sigma} \rangle_{\Omega} = \mathbb{E}^* \langle \boldsymbol{\varepsilon} \rangle_{\Omega}. \quad (38)$$

Because the material is assumed to be macroscopically isotropic it is necessary to determine only two material constants. The most convenient constants are the bulk modulus  $K$  and shear modulus  $G$ , since from (13) we have

$$\langle K \rangle = \frac{\text{tr} \langle \boldsymbol{\sigma} \rangle}{\text{tr} \langle \boldsymbol{\varepsilon} \rangle}, \quad \langle G \rangle = \frac{\text{tr} \langle \boldsymbol{\sigma}^D \rangle}{\text{tr} \langle \boldsymbol{\varepsilon}^D \rangle} \quad (39)$$

**Defining the microstructure.** The fibre-reinforced composite which serves as the model problem consists of a polymer matrix containing thin, randomly orientated, natural-fibre reinforcements. Needle-punching is used to entangle the fibres, which are then bonded into the matrix. This process results in a thin, flat composite which is used as the outer layers in a laminate, which sandwich a honeycomb filler.

Figure 11 shows the entangled fibres, which are of varying length and diameter, of average  $62\text{mm}$  and  $30\mu\text{m}$  respectively, with volume fraction approximately 30%. There is a 50% variation in the diameters of the fibres along their length as a result of their natural origin. Due to the nature of the needle-punching process the fibres are orientated randomly within the matrix.

In order to determine the effective elasticity matrix  $\mathbb{E}^*$ , it is necessary in general to apply six linearly independent loadings defined by linear displacement and constant traction boundary conditions. For a material such as that considered here, which is assumed to be macroscopically isotropic, two constants completely define the macroscopic response, and these can be obtained from a single test. In particular, the two material constants used are the bulk and shear moduli, whose effective values are given by (39).

**Optimal RVE sizing and sampling procedure.** A RVE should capture the nature of the underlying microstructure of the material in question. For an analysis to give accurate material information the RVE would need to be orders of magnitude larger than the length scale of the heterogeneities (the fibres in this case). Practically, however, this is not possible, therefore analyses of two distinct RVEs will yield different results. It is therefore necessary to carry out a number of tests on a range of samples, and obtain an average from the set of results.

The sizing of the RVEs is important; the larger a sample is, the more accurate the information gained from the test. However, a larger sample is also more computationally expensive, thus it is important to find an RVE size that is statistically relevant as well as computationally feasible. For the example studied here the RVE size was estimated by inspection of a scanning electron microscope image (Figure 11) as well as consideration of computational limitations.

The optimal size for the RVE is determined using the following procedure: the geometry of a "large" sample (too large to be computationally feasible) is generated (see Figure 12a). Thereafter a small subdomain within the sample is defined and analysed using the prescribed linear displacement loading condition. The subsample is meshed and tested and the values for the effective bulk and shear moduli ( $K^*$  and  $G^*$  respectively) calculated. The size of the subsample is then increased within the same geometry and tested again (Figure 12a). This process is repeated until the values for  $K^*$  and  $G^*$  converge, at which point the subsample dimensions are used to define the RVE (see Figure 12b). The size of the first subdomain tested is obtained from an inspection of SEM images (Figure 11) and such that it contains the necessary 30% fibre/matrix volume fraction.

**Partitioning of a large sample to find average constitutive values.** Instead of creating many random sample RVEs, one large sample is created and then partitioned into 125 equal sized domains, each one being treated as an RVE, as shown in Figure 12. By solving the boundary value problem on each subdomain  $\Omega_K$  with the linear displacement boundary condition, the effective moduli for the RVE can be obtained as the weighted average of effective moduli for the sub-RVEs.

The material specimen is a cube. Both the polymer matrix and the fibres are assumed to be linear elastic. The fibres (flax in this case) and matrix have Young's moduli  $E$  of 27.6GPa and 1.35GPa respectively, and values of Poisson's ratio  $\nu$  of 0.36 and 0.42 respectively.

The fibres are treated as cylindrical rods of different lengths having an axial stiffness only. The diameter of the fibres is  $30\mu\text{m}$ .

The straight fibres are randomly placed within the matrix. Two points within a domain substantially larger than the RVE size are generated randomly and then joined with a straight line. The generation of the fibres within a domain larger than that of the RVE allows any areas of fibre sparsity around the perimeter of the domain (due to the nature of the randomisation algorithm) to be excluded from the RVE that is analysed. The fibres are

added one at a time and the volume fraction within the RVE is monitored until it reaches 30%.

As there is no specific accommodation on the boundary for a fibre entering/exiting the domain, there is no benefit in having fibres terminating within the domain either. Therefore the fibres are assigned an original length equal to twice the diagonal of the domain. A sphere is generated such that its center is somewhere within the large domain. The points of intersection of the sphere with a random vector passing through its center are the endpoints of the fibre. The fibre is then truncated such that the points of intersection with the boundaries of the domain become its new start and endpoints. Thus the midpoint of the fibre is placed randomly within the domain and the fibre is adjusted to start and end at the boundaries of the domain. Fibres are added until the required volume fraction of 30% is reached. The large domain is then partitioned and the intersections of the fibres with the individual RVE boundaries become the new start and end points for the fibres (for each individual RVE). The data then exists for 125 separate boundary value problems. The algorithm to create the fibre geometries is contained in a Matlab [Mat] code developed for the problem. In developing a finite element analysis of the RVEs, the commercial software, Abaqus [Inc., 2009] is used and the creation of the models is automated using a Python [<http://www.python.org/>.] script developed for the problem.

The fibres are embedded into the matrix using the embedded element constraint in Abaqus. One of the advantages of this constraint is that it allows the fibres to be meshed separately from the matrix; thus the discretisation of the matrix can be regular. This regular mesh is desirable as more control over the element shape is achieved and far fewer degrees of freedom result than from an irregular mesh.

The diameter, and therefore the cross-sectional area, of the fibres is very small in comparison to the size of the RVE. Therefore it is important to have a mesh fine enough to capture the effects of the fibres within the matrix but coarse enough to remain computationally viable.

The partitioning procedure described previously is achieved by retaining the fibre geometry and shifting the subdomain,  $\Omega_K$ , throughout the large domain so that the entire large domain is tested. The results for  $K_K^*$ ,  $G_K^*$  and thus  $\mathbb{E}_K^*$  are calculated and averaged to find  $\tilde{\mathbb{E}}_K^*$ .

The linear displacement loading condition is applied as an essential boundary condition and the results are interrogated for the effective values  $K^*$  and  $G^*$ . The average values,  $\tilde{K}^*$  and  $\tilde{G}^*$  are then calculated.

**Results** The methodology is applied to a sample of  $1\text{cm}^2$ , which is divided into 125 RVEs of  $4\text{mm}^2$  each. The large domain contains 30% fibre volume, with 47,672 fibres randomly dispersed throughout its volume.

One expects effective averaged values to lie somewhere between those of the matrix and the fibres, that is:

$$\Phi_m \leq \tilde{\Phi}^* \leq \Phi_f \quad (40)$$

where  $\Phi$  is the material property in question with subscripts  $m$  for the matrix value and  $f$  for the fibre value. As before,  $\tilde{\Phi}^*$  represents the effective, averaged value for the composite.

The resulting values are given in Table 1. The values show that the inequality in (40) is satisfied except for in the case of Poisson's ratio ( $\nu$ ). As truss elements have no transverse strain, effectively the value used for Poisson's ratio is zero. Therefore the fact that the effective averaged value is below the value for the matrix is acceptable.

Table 1. Material properties

	$\Phi_m$	$\tilde{\Phi}^*$	$\Phi_f$
$K$ (MPa)	1610	2509.21	172500
$G$ (MPa)	496	1001.12	9718
$\mathbb{E}$ (MPa)	1350	2649.76	27600
$\nu$	0.36	0.32	0.42

The histograms in Figures 13 and 14 show the distribution of the results for the 125 sub-domains. These are satisfactory distributions peaking at the average effective values shown in Table 1.

## 5. Open problems and future directions

The objective of this Section is to briefly describe some of the key challenges facing multi-scale modelling methodologies. Issues related to the modelling of fibre-reinforced composites are emphasised. This Section draws heavily on the recent review of Geers et al. [2009] which should be consulted, along with the references therein, for further information.

Standard multi-scale methodologies as presented in this review Chapter have developed significantly over the last 15 years. The method is able to describe the large deformation response of inelastic media with complex microstructure, but certain key limitations exist. One such limitation is the description of shells or plates with complex microstructure which cannot be captured in a layered-wise composite shell approach. Clearly a large number of fibre-reinforced composite products fall into this category. This limitation exists as conventional first-order approximations can not pass second-order information, such as macroscopic deformation gradients (e.g. in bending), to the RVE boundaries. This information is required in shell theory.

A second-order extension of the framework described in this chapter provides a effective way to describe shells with microstructure. The second order methodology also allows for the description of regions of moderate localisation that would otherwise render a first-order approach mesh-dependent and incapable of producing reasonable results. Localisation is typically associated with material regions experiencing intense gradients in deformation, such as occurs during shear banding.

Open questions still exist concerning the extension of the second-order approaches to a range of shell theories and to more general loading conditions. Another key open issue is multi-scale multi-physics coupling. Progress has been made on thermo-mechanical coupling but many other more complex coupling challenges exist (e.g., electro-mechanical, thermo-electrical, fluid-structure interaction, magneto-electro-elasticity, acoustics, amongst others).

From a design point of view it is important to model not only reinforced composites consisting of random arrangements of fibres, but also structured and periodic arrangements such as composites comprising woven fibres [there was a paper along these lines that we looked at some time ago - will try to find it]

In addition, more sophisticated models at the microscopic level would allow a broader range of properties and phenomena to be captured. For example, viscoelastic effects are important in some situations, and depending on the fibrous material, damage as a result of fibre breakage would in certain situations be an important consideration. Furthermore, in the examples treated in this chapter perfect bonding between fibre and matrix has been assumed; it would be important to model, and hence to gain a better understanding of the conditions under which debonding takes place, and its effect on the overall, macroscopic material properties.

## Acknowledgements

A large portion of the work presented in this chapter forms part of a project in collaboration with the Council for Scientific and Industrial Research (CSIR), and forms part of an overarching project Natfibio: Development of a natural fibre/bio-composite cabin interior component, sponsored jointly by Airbus, the Department of Science and Technology, and the Advanced Manufacturing Technology Strategy. The cooperation and contributions of Drs R Anandjiwala and A Patnaik are gratefully acknowledged.

The considerable contributions from Helen Morrissey at the Centre for Research in Computational and Applied Mechanics at the University of Cape Town and Hellmut Bowles from Finite Element Analysis Services are greatly appreciated.

## References

- V. Belsky, M. W. Beall, J. Fish, M. S. Shephard, and S. Goma. Computer-aided multiscale modelling tools for composites materials and structures. *Computing Systems in Engineering*, 6(3):213–223, 1995.
- F. Feyel. Multiscale  $FE^2$  elastoviscoplastic analysis of composite structures. *Computational Materials Science*, 16:344–353, 1999.
- F. Feyel and J.-L. Chaboche.  $FE^2$  multiscale approach for modelling the elastoviscoplastic behaviour of long fibre SiC/Ti composite materials. *Computer Methods in Applied Mechanics and Engineering*, 183:309–330, 2000.
- M. G. D. Geers, V. G. Kouznetsova, and W. A. M. Brekelmans. Multi-scale computational homogenization: Trends and challenges. *Journal of Computational and Applied Mathematics*, 2009. doi: doi:10.1016/j.cam.2009.08.077.
- C. González and J. LLorca. Multiscale modeling of fracture in fiber-reinforced composites. *Acta Materialia*, 54:4171–4181, 2006.

R. Hill. The elastic behaviour of a crystalline aggregate. *Proceedings of the Physical Society of London*, A65:349–354, 1952.

<http://www.python.org/>. URL <http://www.python.org/>.

T. J. R. Hughes. *The Finite Element Method. Linear Static and Dynamic Finite Element Analysis*. Prentice–Hall, Englewood Cliffs, N. J., 1987.

ABAQUS Inc. *ABAQUS/Standard, ABAQUS Analysis User's Manual. Version 6.8*. Simulia, Providence, RI, 2009.

V. Kouznetsova. *Computational homogenization for the multi-scale analysis of multi-phase materials*. PhD thesis, Eindhoven University of Technology, 2002.

F. Maceri, M. Marino, and G. Vairo. A unified multiscale mechanical model for soft collagenous tissues with regular fiber arrangement. *Journal of Biomechanics*, 43:355–363, 2010.

P. K. Mallick. *Fiber-reinforced composites: materials, manufacturing, and design*. Marcel Dekker, Inc, 2nd edition, 1993.

I. Ozdemir, W. A. M. Brekelmans, and M. G. D. Geers.  $FE^2$  computational homogenization for the thermo-mechanical analysis of heterogeneous solids. *Computer Methods in Applied Mechanics and Engineering*, 198:602–613, 2008.

V. Sansalone, P. Trovalusci, and F. Cleri. Multiscale modeling of materials by a multifield approach: Microscopic stress and strain distribution in fiber-matrix composites. *Acta Materialia*, 54:3485–3492, 2006.

Z. Xia, W. A. Curtin, and P. W. M. Peters. Multiscale modeling of failure in metal matrix composites. *Acta Materialia*, 49:273–287, 2001.

Z. H. Xia and W. A. Curtin. Multiscale modeling of damage and failure in aluminum-matrix composites. *Composites Science and Technology*, 61:2247–2257, 2001.

O. C. Zienkiewicz and R. L. Taylor. *The Finite Element Method for Solid and Structural Mechanics*. Elsevier Butterworth-Heinemann, 2005.

T. I. Zohdi and P. Wriggers. Aspects of the computational testing of the mechanical properties of microheterogeneous material samples. *International Journal for Numerical Methods in Engineering*, 50:2573–2599, 2001.

T.I. Zohdi and Peter Wriggers. *Introduction to Computational Micromechanics (Lecture Notes in Applied and Computational Mechanics)*. Springer-Verlag New York, Inc., Secaucus, NJ, USA, 2004.

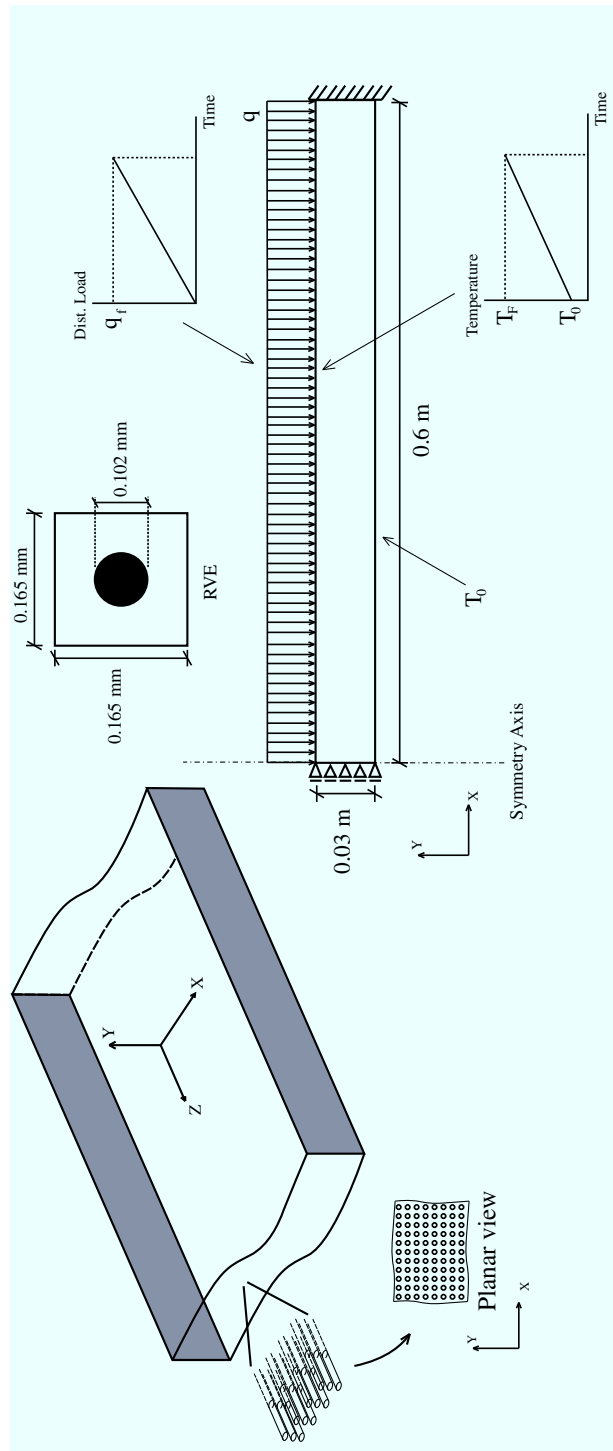


Figure 1. Thermo-mechanically loaded plate; geometry, boundary conditions and RVE (from [Ozdemir et al., 2008])

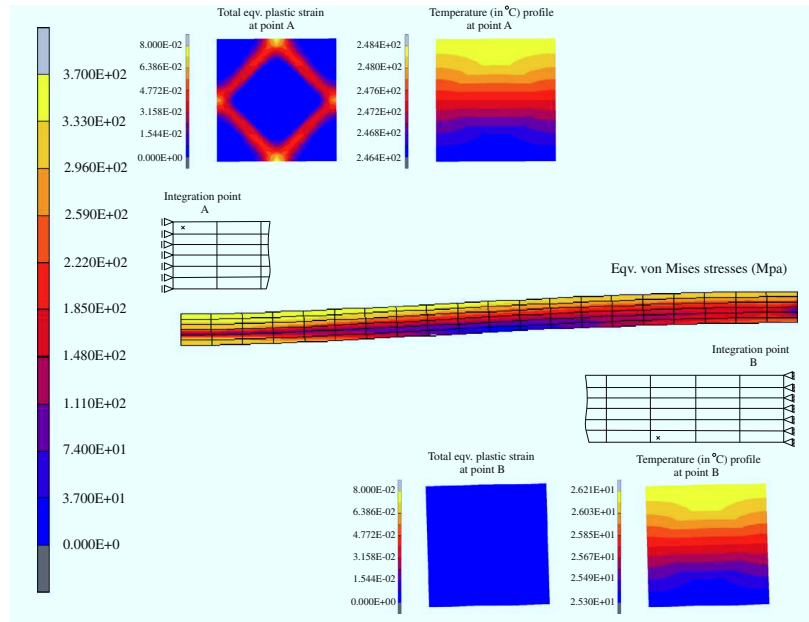


Figure 2. Two-scale solution via computational homogenisation at  $t = 10.0$  s. (from [Ozdemir et al., 2008])

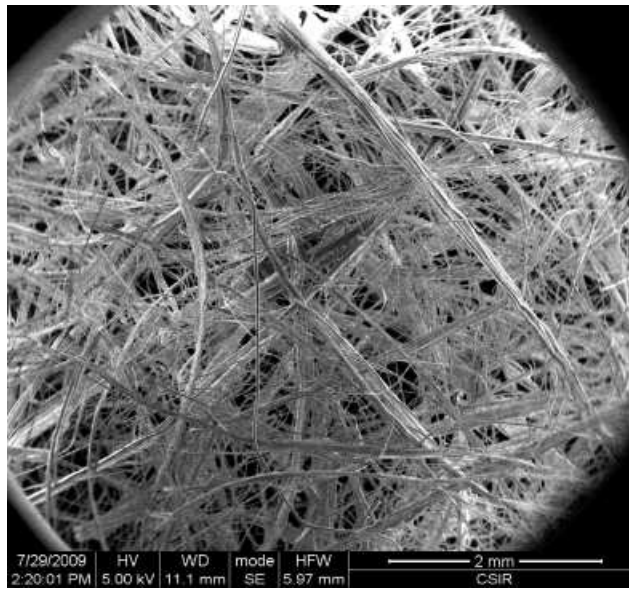


Figure 3. Scanning electron microscope image of a randomly distributed fibre network. (Image courtesy of the Council for Scientific and Industrial Research (CSIR), Port Elizabeth)

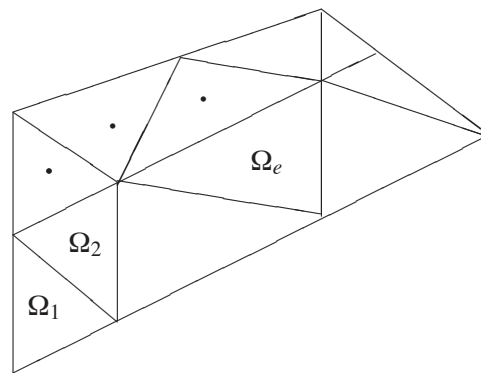


Figure 4. A polygonal domain in  $\mathbb{R}^2$  and its subdivision into finite elements

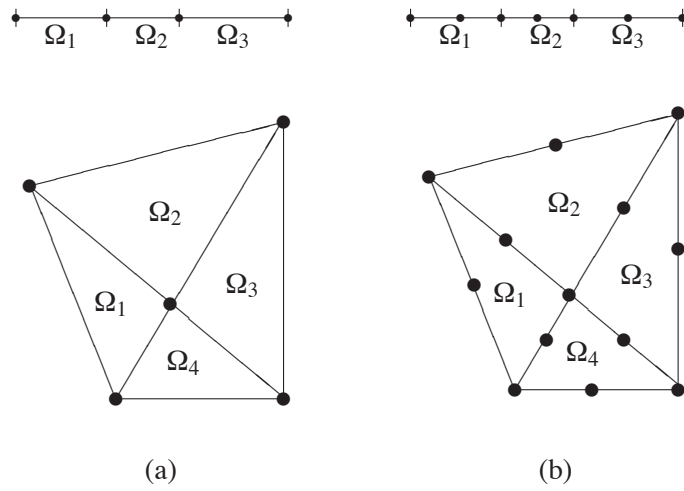


Figure 5. Finite element meshes comprising elements and nodal points

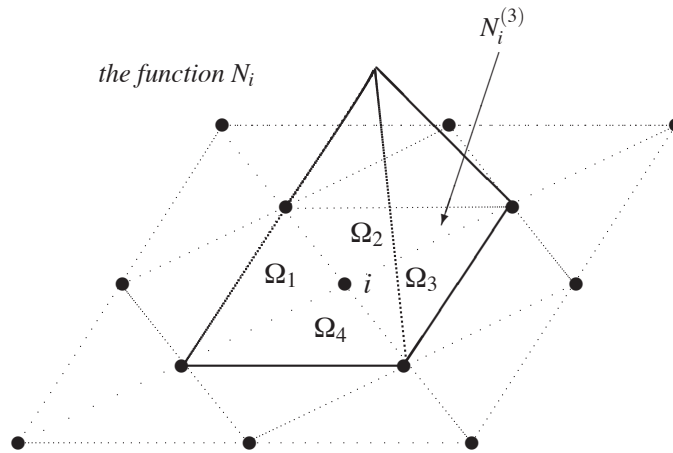


Figure 6. Local and global shape functions

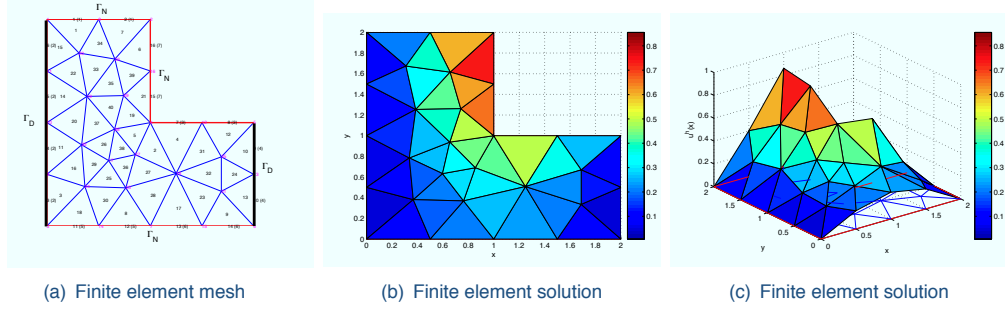


Figure 7. A finite element mesh and piecewise-linear solution

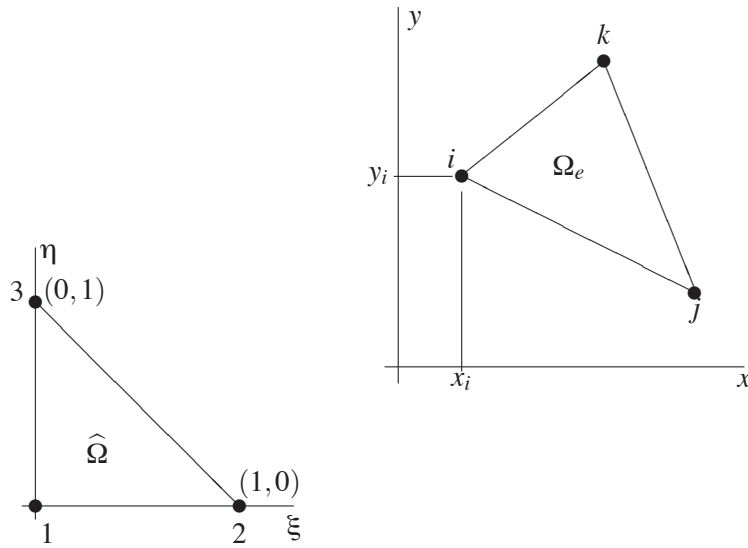


Figure 8. A triangular element and the corresponding reference element

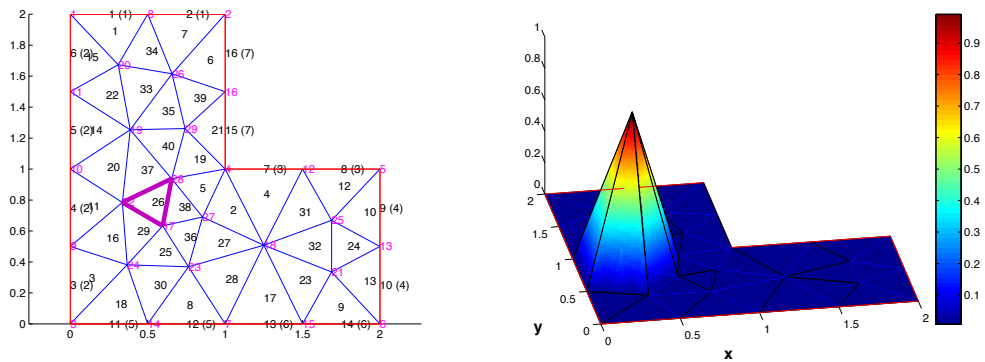


Figure 9. A mesh in 2D and a typical global shape function

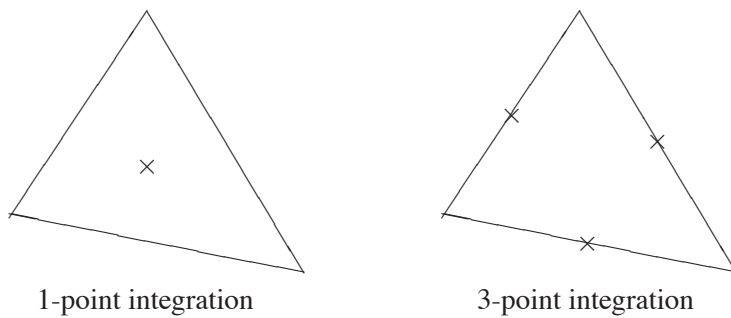


Figure 10. Integration rules on the reference triangle

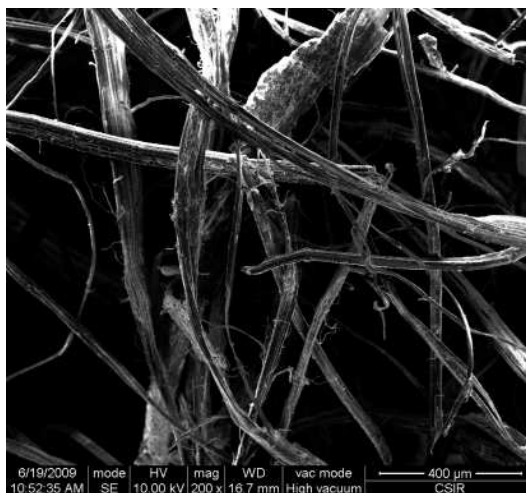


Figure 11. Scanning electron microscope image of the entangled fibres. (Image courtesy of the Council for Scientific and Industrial Research (CSIR), Port Elizabeth)

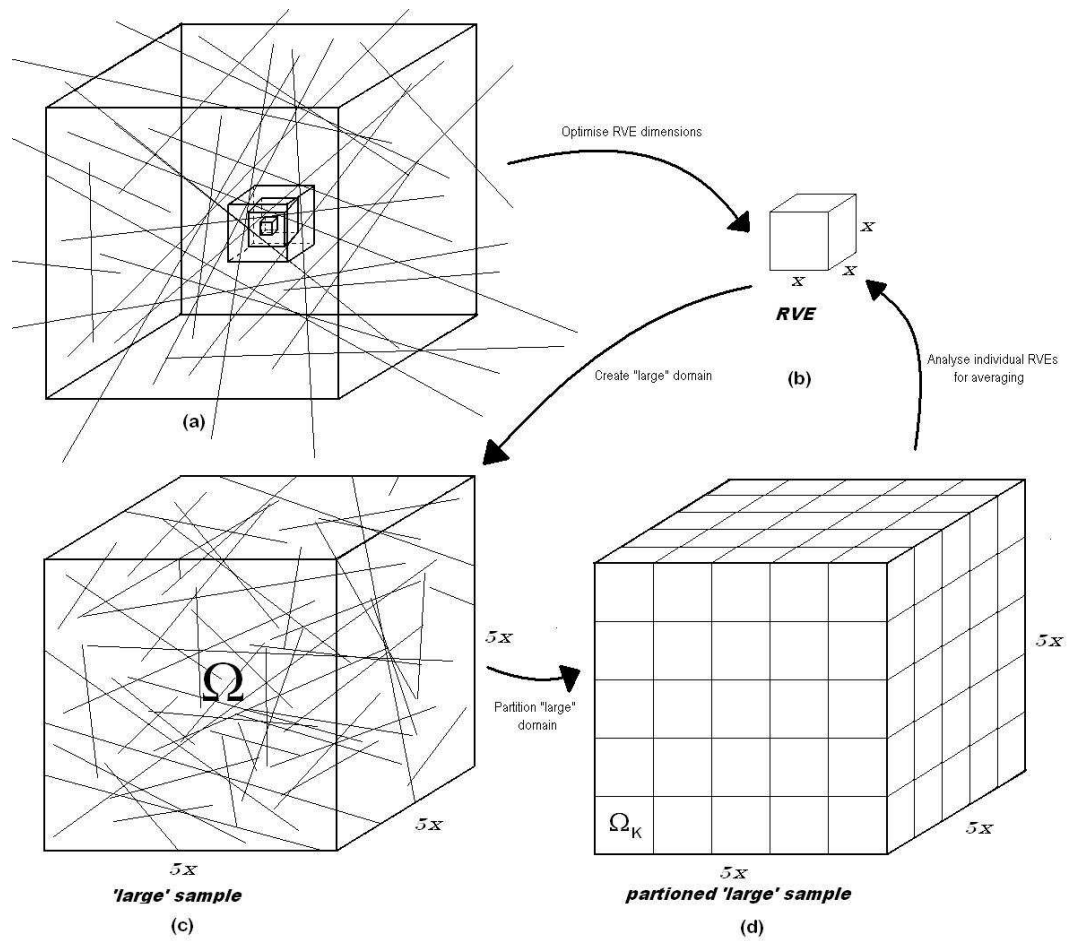


Figure 12. Testing methodology to find RVE size and test multiple samples by partitioning a "large" domain

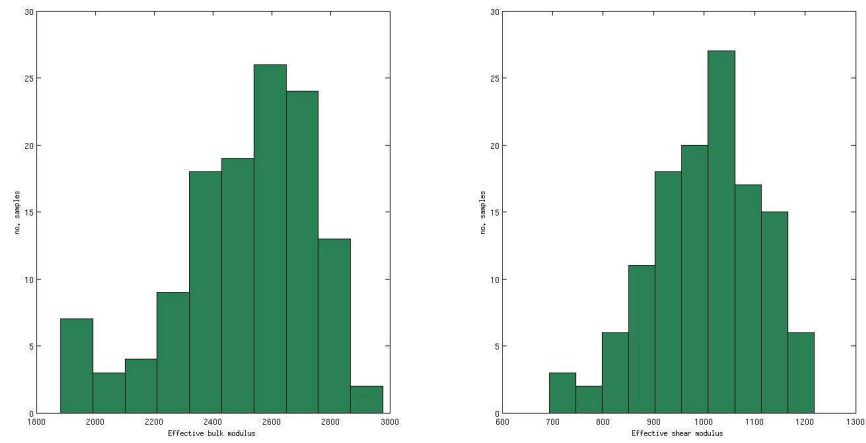


Figure 13. Distribution of data for effective bulk and shear moduli

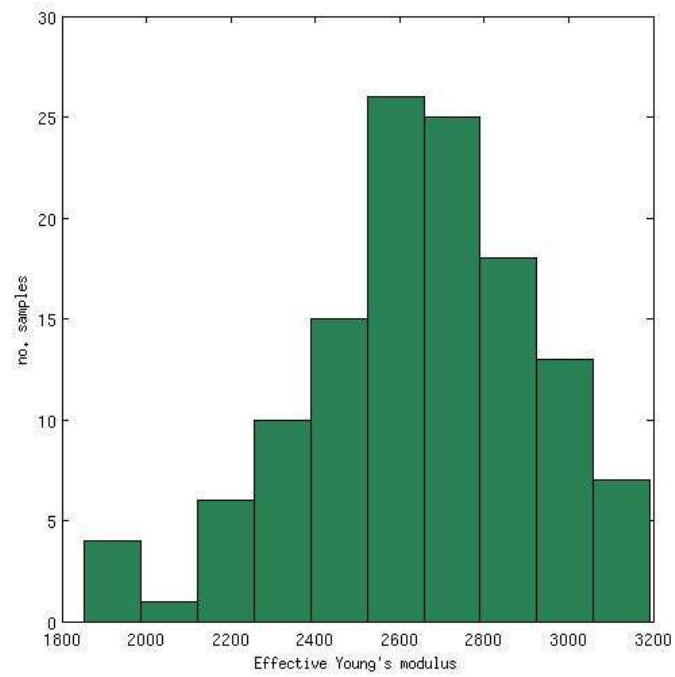


Figure 14. Distribution of data for effective Young's modulus